

Magnetic anisotropy and magnetic phase diagram of Gd₅Ge₄

Z. W. Ouyang

Materials and Engineering Physics Program, Ames Laboratory, Iowa State University, Ames, Iowa 50011-3020, USA

V. K. Pecharsky* and K. A. Gschneidner, Jr.

*Materials and Engineering Physics Program, Ames Laboratory, Iowa State University, Ames, Iowa 50011-3020, USA
and Department of Materials Science and Engineering, Iowa State University, Ames, Iowa 50011-2300, USA*

D. L. Schlagel and T. A. Lograsso

*Materials and Engineering Physics Program, Ames Laboratory, Iowa State University, Ames, Iowa, 50011-3020, USA
(Received 11 January 2006; revised manuscript received 30 May 2006; published 5 July 2006)*

The magnetization of single crystal Gd₅Ge₄, which in a zero magnetic field orders antiferromagnetically at 128 K, indicates a reversible spin-flop transition when the magnetic field is along the *c* axis and the absence of similar transformations when the magnetic field vector is perpendicular to the *c* axis. This anisotropic behavior is due to variation of magnetization energy between the *c* axis and the *a* or *b* axes of the orthorhombic crystal caused by a different alignment of the Gd moments with respect to the magnetic field vector. The anisotropy of the antiferromagnetic state diminishes with the increasing magnetic field and temperature. The critical magnetic field for the antiferromagnetic-ferromagnetic transition is the smallest and the ferromagnetic state is most stable when the magnetic field vector is parallel to the *b* axis, indicating an easy magnetization direction along this axis. The anisotropy of the magnetic field-induced transformation in Gd₅Ge₄ is discussed in connection with the coupled magnetic and structural transitions. Anisotropic magnetic phase diagrams along the three major crystallographic axes are constructed.

DOI: [10.1103/PhysRevB.74.024401](https://doi.org/10.1103/PhysRevB.74.024401)

PACS number(s): 75.30.Gw, 75.30.Kz, 75.50.Ee, 75.50.Cc

I. INTRODUCTION

Magnetic anisotropy is an important and intrinsic property of many rare-earth-based magnetic materials.¹⁻⁴ The varying levels of anisotropy in these compounds are related to single ion anisotropies of specific lanthanide ions and/or to the anisotropy of the crystal lattice resulting from a particular crystal structure, often distinctly layered. The nonzero magnetic anisotropy of Gd-based compounds receives considerable attention because the Gd³⁺ ion has a negligible anisotropy of its 4*f*-electron wave functions and anisotropic magnetic properties are defined solely by the crystal lattice.^{5,6}

The pseudobinary Gd₅Si_{*x*}Ge_{4-*x*} compounds, as a recent example of naturally layered materials, exhibit unusually strong responses to small changes of magnetic field, such as large magnetocaloric, magnetostrictive, and magnetoresistance effects when *x* ≤ ~2.⁷⁻¹¹ Early experiments revealed that they are due to the magnetic field-induced first-order magnetic phase transition which in these compounds is accompanied by a simultaneous crystallographic transformation.^{9,12} These coupled magneto-structural transitions, depending on the value of *x*, magnetic field, temperature, and pressure,¹³⁻¹⁵ were found to be related to the breaking or the reforming of (Si, Ge)-(Si, Ge) covalentlike bonds between structurally well-defined, subnanometer-thick slabs that are infinite in two dimensions along the *a* and *c* axes and are stacked differently along the *b* axis forming three different crystal structures found in the Gd₅Si_{*x*}Ge_{4-*x*} family.^{12,16} Despite the distinctly anisotropic crystal lattices, little is known about the related anisotropy of the physical behaviors in the Gd₅Si_{*x*}Ge_{4-*x*} system.

One of the parent compounds, Gd₅Ge₄, is especially intriguing because of its peculiar magnetic properties that are

clearly related to instability of the crystal structure of the material. The magnetic ground state of Gd₅Ge₄ is believed to be antiferromagnetic (AFM).¹⁷⁻²⁰ The AFM state can be transformed into the ferromagnetic (FM) state depending on the temperature and the applied magnetic field as long as the latter exceeds ~10 kOe. At the same time, the crystal structure is transformed from the Sm₅Ge₄-type to the Gd₅Si₄-type structure, with the transition showing a martensiticlike character.^{21,22} Below ~10 K, the magnetic-field-induced AFM-FM transition in polycrystalline Gd₅Ge₄ is irreversible, while above ~20 K the transition becomes completely reversible. Between ~10 and ~20 K, there exists a mixture of states exhibiting both irreversible and reversible AFM-FM transitions.^{18,23,24} It appears that the unusual magnetic correlations in Gd₅Ge₄ originate from the anisotropy of exchange interactions that arises from the presence of the distinctly two-dimensional slabs exhibiting varying interslab interactions and bonding.

A few basic magnetic properties of a Gd₅Ge₄ single crystal were recently investigated.²⁵ It was postulated that below the Néel temperature, the magnetic moments of Gd are ferromagnetically coupled within each slab but the slabs are antiferromagnetically coupled along the *c* axis in low magnetic fields (*H* ≤ ~8 kOe). This assumption was supported by a recent microscopic study of the magnetic structure of a single crystal of Gd₅Ge₄ performed by x-ray resonant magnetic scattering measurements.²⁶ Interestingly, a fully reversible spin-flop transition was observed at 4.3 K when a magnetic field of ~8.4 kOe was applied along the *c* direction.²⁵ To date, data about anisotropy of the magnetic properties of Gd₅Ge₄ are limited to Ref. 25 which reports isothermal magnetization at 4.3 K and isofield magnetization in several fixed magnetic fields.

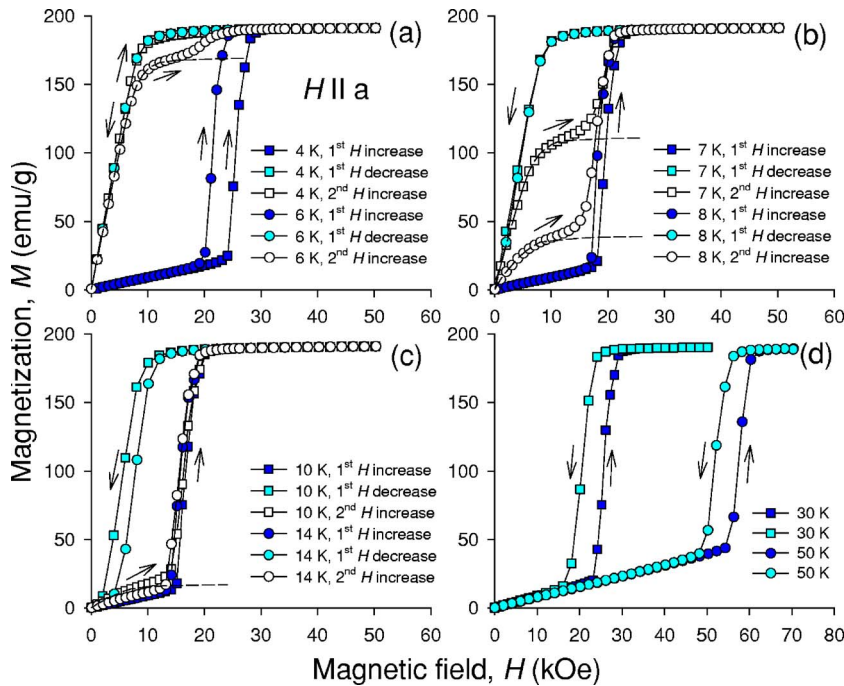


FIG. 1. (Color online) The magnetic field dependencies of the magnetization of the ZFC single crystal of Gd_5Ge_4 measured when the magnetic field vector is parallel to the a axis. The dashed lines show the extrapolated magnetic behavior without the magnetic field-induced AFM-FM transition during the second field-increasing measurement.

In this work, we study details of the magnetic anisotropy by both the isothermal $M(H)$ and isofield $M(T)$ measurements along the three principal axes of the crystal. Since the ground state of Gd_5Ge_4 is an antiferromagnet, we examine both the anisotropy of the AFM state and the anisotropy of the magneto-structural transition. Finally, the magnetic phase diagrams with the magnetic field vector applied along the three principal crystallographic axes are constructed.

II. EXPERIMENTAL DETAILS

A single crystal of Gd_5Ge_4 was grown using the tri-arc pulling technique starting with a polycrystalline ingot with the same nominal chemical composition.²⁷ Polycrystalline Gd_5Ge_4 was prepared by arc melting stoichiometric amounts of high purity Gd and Ge metals under an argon atmosphere. The gadolinium metal (99.9 at. % pure) was obtained from the Ames Laboratory Materials Preparation Center²⁸ and contained the following major impurities (in parts per 10^6 atomic): O, 440; C, 200; H, 160; N, 90; Fe, 40; and F, 30. The Ge metal was better than 99.99 at. % pure and it was purchased from Meldform Metals, Inc. The ingot was flipped and melted several times to ensure homogeneity. The arc melted button was used as the charge material in a tri-arc furnace. A tungsten rod was used as the seed material, which resulted in a randomly oriented Gd_5Ge_4 crystal. The as-grown single crystal was oriented by back-reflection Laue x-ray diffraction and a cubelike sample with its faces parallel to the (100), (010), and (001) crystallographic planes was cut from a large single crystalline grain by the spark erosion technique. Final dimensions of the sample were $1.22 \times 1.23 \times 1.30 \text{ mm}^3$.

The magnetization measurements were performed in a commercial (Quantum Design) superconducting quantum interference device (SQUID) magnetometer, model MPMS-

XL, over a temperature range of 2–300 K and a magnetic field range of 0–70 kOe. Each measurement sequence was recorded after the sample was zero field cooled (ZFC) from the paramagnetic (PM) state at 300 K. In the ZFC isothermal $M(H)$ scans, the first measurement includes the first field increase and the subsequent field reduction. The second field increase was performed immediately after the first measurement. During the measurements, the deviation of the alignment of the magnetic field vector with the crystallographic directions of the single crystal was less than $\sim 5^\circ$.

III. EXPERIMENTAL RESULTS

Figures 1 and 2 show the isothermal magnetization curves of the ZFC Gd_5Ge_4 single crystal measured with the magnetic field vector parallel to the crystallographic a , and c axes, respectively (magnetization data along the b axis are similar to those shown in Fig. 1, the major differences are slightly lower critical magnetic fields and narrower hysteresis at 30 K and 50 K). The $M(H)$ curves exhibit the AFM-FM transition similar to that reported for polycrystals.^{17,18,20,23} In polycrystalline samples, however, the field-increasing branches of the ZFC $M(H)$ curves measured below ~ 9 K present two metamagnetic features, as illustrated in Fig. 3, for two different specimens. The first is usually observed as a nearly discontinuous transition (e.g., at ~ 17 kOe for 6.1 K isotherm) and the second is a continuous one, which occurs near the saturation of the magnetization (e.g., between ~ 18 kOe and 25 kOe for the 6.1 K isotherm). We note that a similar continuous transition in addition to a sharp metamagnetic-like feature was observed in polycrystalline Gd_5Ge_4 by Hardy *et al.*,²⁹ but the origin of the anomaly was left without a discussion. Such a two-step metamagnetic transition is quite unusual and is obviously an intrinsic property of polycrystalline Gd_5Ge_4 regardless of the source of the

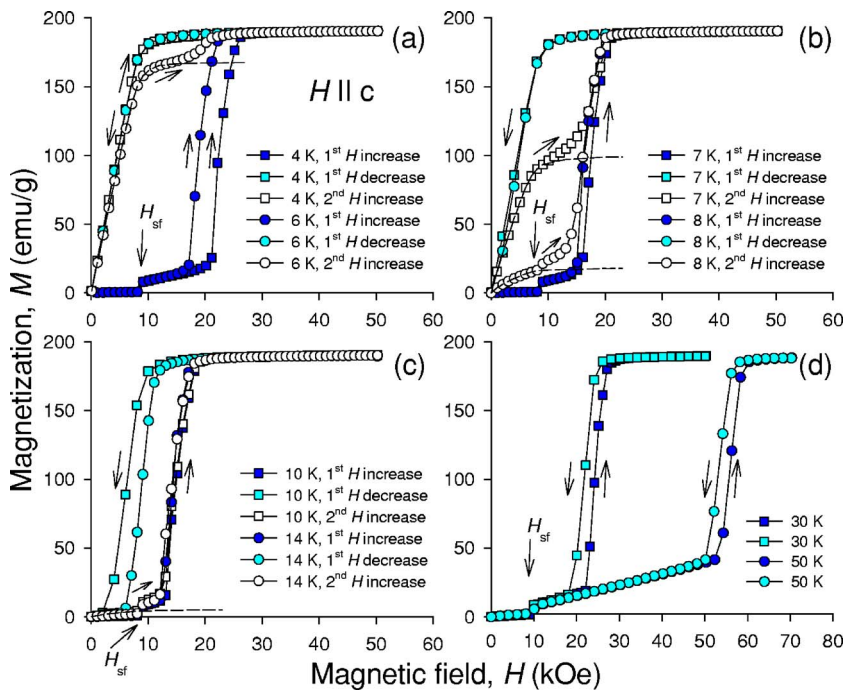


FIG. 2. (Color online) The magnetic field dependencies of the magnetization of the ZFC single crystal of Gd_5Ge_4 measured when the magnetic field vector is parallel to the c axis. The dashed lines show the extrapolated magnetic behavior without the magnetic field-induced AFM-FM transition during the second field-increasing measurement. The arrows marked H_{sf} point to the anomalies associated with a spin-flop transition.

material (the two samples from Fig. 3 have been prepared from high purity Gd,²⁸ while the sample in Ref. 29 was made using commercial, “99.9% pure” Gd metal). At $T \geq 9.7$ K, the second feature on the $M(H)$ curves disappears. We believe that either of the two following mechanisms may be responsible for the differences in the behaviors of M with H in a single crystal and in a polycrystal. First, the tail-like metamagnetic features in polycrystalline samples may be related to kinetic arrest of the first-order magneto-structural transition.³⁰ As temperature increases to ~ 10 K, thermal energy overcomes kinetic limitation and the high-field tail gradually disappears. Second, as seen in Figs. 1 and 2, the critical magnetic fields, H_{cr} , are different for different crystallographic directions. Furthermore, H_{cr} are temperature dependent and the rates of their change with temperature are also different. Thus, the high-field $M(H)$ tails observed immediately after the sharp steps in the polycrystal data (Fig. 3) may be reflective of the magnetocrystalline anisotropy of Gd_5Ge_4 coupled with a complex preferred orientation of the grains in the as-solidified arc-melted buttons.

A. Anisotropy of the AFM state

The anisotropy of the AFM state of Gd_5Ge_4 is marked first by a spin-flop transition observed along the c axis. The magnetization increases nearly linearly for the a and b axes with increasing magnetic field regardless of temperature, but the magnetic behavior along the c axis is quite different. A nearly discontinuous steplike transition is observed at various temperature-dependent critical fields H_{sf} . On both sides of H_{sf} , the magnetization along the c axis varies linearly but with a different slope. Below H_{sf} , the slope is much smaller, indicating a more complete compensation of the magnetic moments. This picture agrees with a model where the antiferromagnetic coupling of the Gd moments occurs along the c axis, as suggested in Refs. 25 and 26. The temperature

behaviors of H_{sf} and dc magnetic susceptibility in the AFM state are illustrated in Figs. 4 and 5. The critical field H_{sf} increases nonlinearly from ~ 8.3 kOe at 2 K and then saturates at 10.3 kOe between 80 K and 128 K. With increasing temperature, dM/dH increases before and decreases after the spin-flop transition, leading to a gradual reduction of the step at H_{sf} . The $M(H)$ discontinuity becomes a minor slope

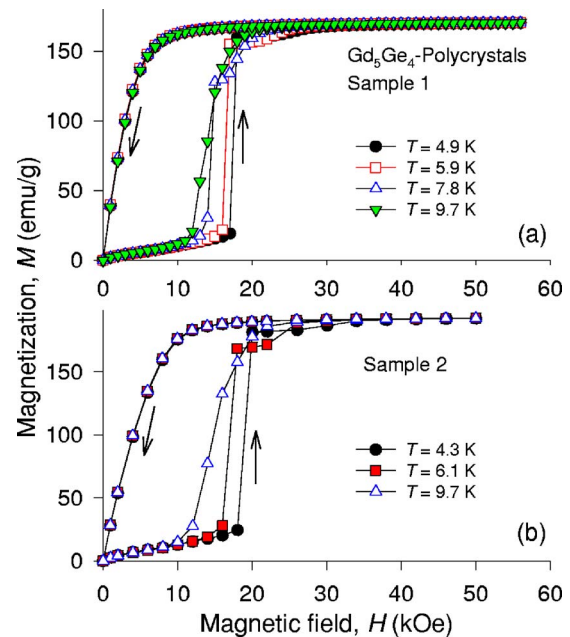


FIG. 3. (Color online) The magnetic field dependencies of the magnetization of two different ZFC polycrystalline Gd_5Ge_4 samples measured at nearly the same temperatures. The data for sample 1 are taken from Ref. 23; the magnetization data of sample 2 were measured in an extraction magnetometer (Lake Shore) using a piece of a different arc-melted alloy button with the same nominal composition.

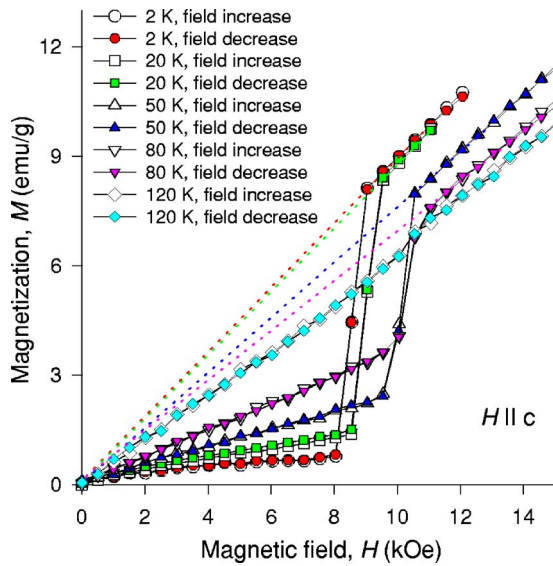


FIG. 4. (Color online) The field dependencies of the magnetization of the ZFC Gd_5Ge_4 single crystal measured at different temperatures when the magnetic field vector is parallel to the c axis. The dotted lines represent linear extrapolations of the $M(H)$ behavior above the spin-flop transition to a zero magnetic field.

change at $T=120$ K and it disappears above $T_N \cong 128$ K. Extrapolating the M vs H behavior above H_{sf} to $H=0$ (dotted lines in Fig. 4) shows that M approaches zero as H approaches zero, and therefore, the magnetic structure remains AFM with a nearly zero spontaneous magnetization but with a larger magnetic susceptibility when compared to the normal AFM Gd_5Ge_4 (i.e., the zero magnetic field state of the compound). The $M(H)$ curves for both the field-increasing and the field-decreasing branches coincide with each other, showing that the field-induced spin-flop transition is fully reversible and nonhysteretic. We note that in the second H -increasing measurement, the spin-flop transition along the c axis is only observed above 7 K (see Fig. 2).

The anisotropy of the AFM state is also manifested in the isofield magnetization data. Figure 6 shows the ZFC heating and field cooling (FC) $M(T)$ curves measured both in low [$H=0.5$ kOe, 3 kOe, and 10 kOe, Figs. 6(a)–6(c)] and high fields [$H=20$ kOe and 50 kOe, Figs. 6(d)–6(f)]. An AFM-PM transition is observed along all three axes at T_N . With decreasing temperature, the $M(T)$ curves exhibit a profound anisotropy in low magnetic fields. No states other than the normal AFM Gd_5Ge_4 are observed in the 0.5 kOe and 3 kOe $M(T)$ curves. The same is true for the 10 kOe applied field along the a axis, where a kink is observed at ~ 14 K, below which the ZFC and FC $M(T)$ curves diverge slightly [Fig. 6(a)]. The c -axis $M(T)$ curve [Fig. 6(c)] exhibits a reversible spin-flop transition at ~ 50 K and a kink at ~ 14 K, which is similar to that observed along the a axis in Fig. 6(a). When a 10 kOe magnetic field is applied along the b axis [Fig. 6(b)], Gd_5Ge_4 is no longer in a purely AFM state. The magnetic field dependence of the spin-flop transition is further illustrated in more detail in Fig. 7, in which the 0.5, 3, and 10 kOe data from Fig. 6 are also included.

With the occurrence of the spin-flop transition, Gd_5Ge_4 exhibits at least two distinct AFM states (see Figs. 4 and 7).

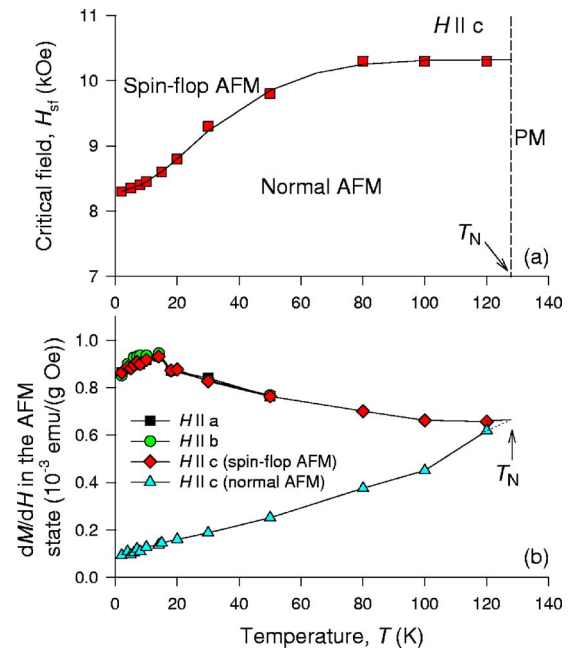


FIG. 5. (Color online) (a) The temperature dependence of the critical field H_{sf} for the spin-flop transition. (b) The temperature dependencies of the slopes of the $M(H)$ curves (dM/dH) in the AFM state.

When $H < 8.3$ kOe, the “normal” AFM state is stable at all temperatures below T_N . When $H > 10.3$ kOe is applied along the c axis, the spin-flop AFM structure exists in the same temperature range and when $8.3 \text{ kOe} < H < 10.3$ kOe, the stability of either state becomes temperature dependent. As deduced from the results presented in Figs. 4 and 7, the magnetic moments of Gd below 128 K are coupled antiferromagnetically along the c axis when the applied field is below 8.3 kOe. With the spin-flop transition, the AFM coupling of the Gd magnetic moments changes its direction from parallel to perpendicular to the c axis.

To explore the details of the anisotropy of the AFM state, the 0.5 kOe ZFC and FC $M(T)$ curves are shown together in Fig. 8(a). We note that the FC $M(T)$ curves diverge from the ZFC curves below ~ 60 K for the a and c axes, and below ~ 40 K for the b axis. On the other hand, the $H=3$ kOe and higher field $M(T)$ curves follow one another closely as long as Gd_5Ge_4 remains AFM for both ZFC and FC states down to ~ 14 K, below which they become slightly divergent (also see Fig. 6). Furthermore, when the magnetic field is parallel to the a or the b axis, the magnetization in the AFM state decreases with increasing temperature. Chattopadhyay *et al.*³¹ report a similar behavior for a polycrystalline sample, attributing this to spin fluctuations and FM correlations apparently present in the sample. The 0.5 kOe $M(T)$ curves for the a and b axes diverge below T_N [see Fig. 8(a)], which is different from the 8 kOe data of Ref. 25 and from our data above 3 kOe [Fig. 8(b)] indicating that the $M(T)$ curves in the AFM state above 3 kOe always nearly overlap for the a and b axes. That is, the anisotropy of the AFM state between the a and the b axes at low temperatures and low fields is weak, and a 3 kOe field is high enough to completely

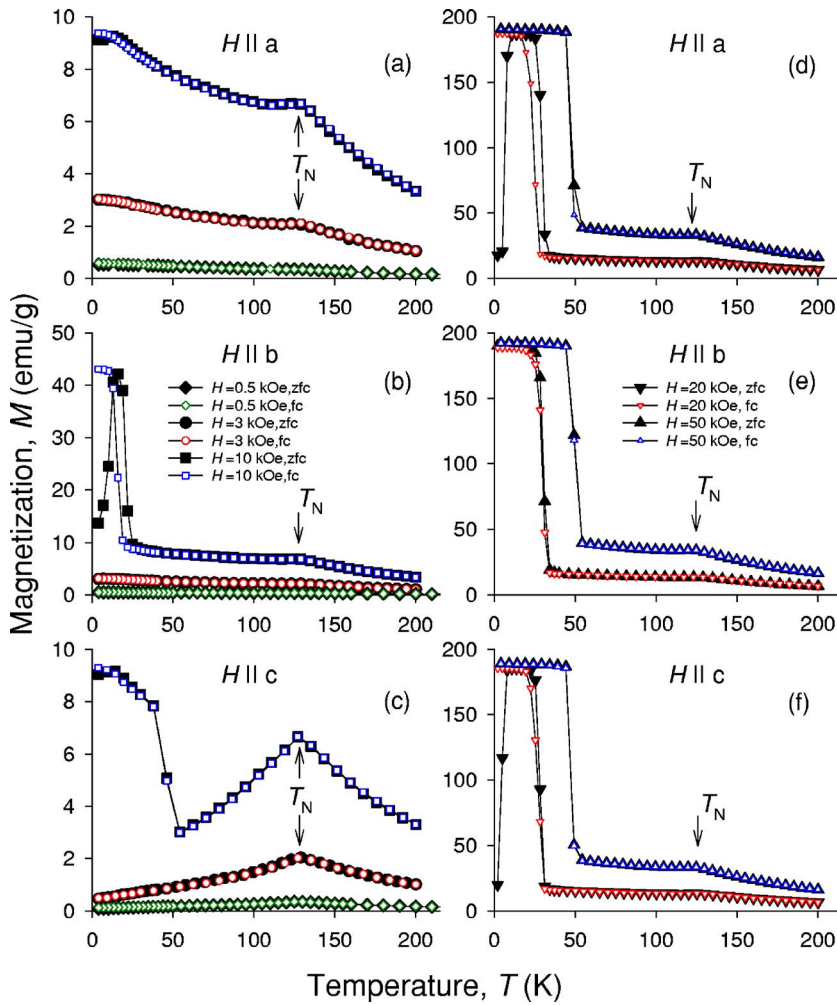


FIG. 6. (Color online) The ZFC heating (solid points) and FC $M(T)$ curves (open points) of the single crystal of Gd_5Ge_4 measured at $H=0.5$ kOe, 3 kOe, and 10 kOe [(a), (b), and (c)] and $H=20$ kOe and 50 kOe [(d), (e), and (f)] with the magnetic field vector parallel to the a , b , and c axes.

suppress this anisotropy. When the field vector is applied along the c axis, the magnetization increases with increasing temperature, resembling the earlier reported results.²⁵ Extrapolating the 0.5 kOe $\mathbf{H} \parallel c$ $M(T)$ curve to zero temperature, suggests that the magnetization remains larger than zero due to the incompletely compensated moments. A similar conclusion can be drawn from the 0.1 kOe data reported in Ref. 26. The difference of the magnetization between the c axis and the other two axes, as shown in the inset of Fig. 8(a), varies almost linearly below T_N , indicating that the anisotropy in the AFM state increases nearly linearly with decreasing temperature.

The magnetic anisotropy in the AFM state observed in the isothermal $M(H)$ and isofield $M(T)$ measurements can be understood by considering the configuration of Gd moments with respect to the external magnetic field. When the magnetic field is parallel to the a or b axis, the spin axis of the Gd moments (i.e., the c axis) is perpendicular to the field vector. Thus, the magnetization decreases with increasing temperature as follows from Néel's model³² and from possible FM spin fluctuations in the sample. However, when the field vector is applied along the c axis, the spin axis of the Gd moments is also parallel to the field vector. This AFM state is denoted as the normal AFM state because of its similarity to the classical magnetic behavior of an antiferromagnet [see Fig. 8(a)]. Since the magnetic susceptibility along

the a axis, χ_a (or the b axis, χ_b), is always larger than that along the c axis, χ_c , the energy of magnetization below T_N given by $E = -(1/2)\chi H^2$ is always lower for the a axis or b axis than for the c axis. The thermodynamically stable system must have the lowest magnetic energy, and therefore, the whole spin arrangement along the c axis tends to rotate so as to make its spin axis perpendicular to the external field. Néel³² predicted that such a flopping of the spin axis should occur when the field reaches some critical value. The critical field is determined by the magnitude of the magnetocrystalline anisotropy. For the present sample, the required critical field lies between ~ 8.3 kOe and ~ 10.3 kOe for $2 \text{ K} < T < T_N$. Accordingly, the directions of the Gd moments in the spin-flop AFM state (within the ab plane) are perpendicular to the magnetic field vector (i.e., the c axis). The magnetic behavior of the spin-flop AFM state is therefore expected to be similar to that along the a and b axes [see Figs. 5(b) and 8(b)], where the magnetic field vector is also perpendicular to the directions of the Gd moments. Therefore, the AFM state anisotropy is considerable only at low temperatures and in low magnetic fields. Raising the temperature and the magnetic field decreases the differences in the magnetic energy between the a axis (and the b axis) and the c axis, and therefore, reduces the magnetocrystalline anisotropy of the compound in the AFM state.

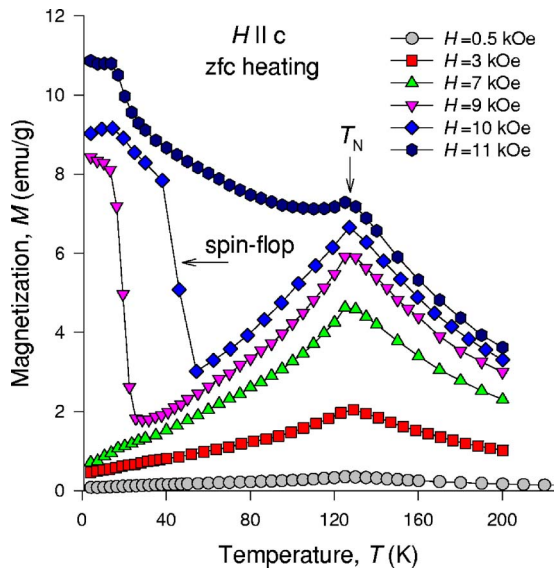


FIG. 7. (Color online) The ZFC heating $M(T)$ curves of Gd_5Ge_4 single crystal measured when the magnetic field vector is parallel to the c axis.

B. Anisotropy of the AFM-FM transition in Gd_5Ge_4

The anisotropy of the magnetic field-induced AFM-FM transition is prominent. As shown in Figs. 1 and 2, the field induced AFM-FM transition is not as sharp as one might expect for a single crystal, i.e., it starts at a certain critical field H_{c1} and ends at a higher critical field H_{c2} . The critical fields decrease with increasing temperature, reaching directionally dependent minima at ~ 14 K, and above this temperature, both H_{c1} and H_{c2} begin to increase with temperature (see Fig. 9). The values of the critical fields vary with the crystallographic directions. Between 2 K and 50 K, the values of H_{c1} and H_{c2} for the b axis are notably lower than those for the c axis, and the latter are lower than those along the a axis. The minimum of H_{c1} and H_{c2} along the b axis indicates that the compound is more easily converted into the FM state with field applied in this direction compared with the other two axes. The difference between the critical fields along different axes is large at low temperature, gradually diminishing as temperature rises, indicating the reduction of the magnetocrystalline anisotropy.

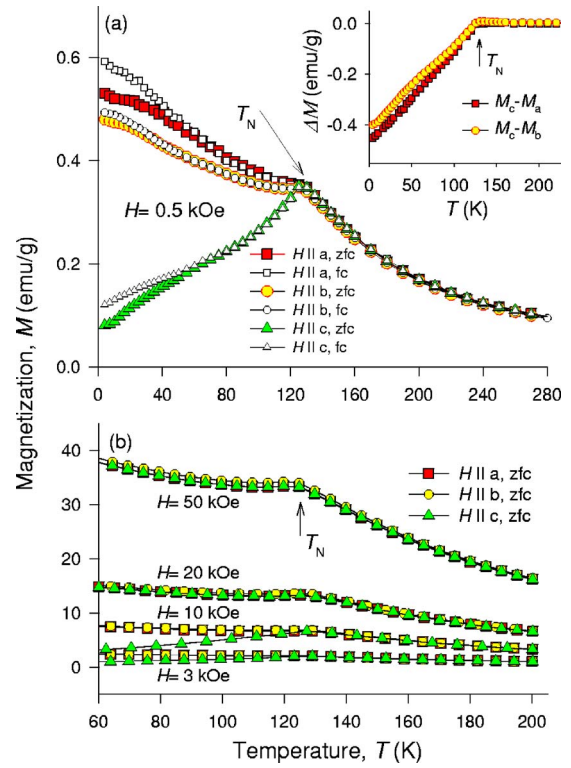


FIG. 8. (Color online) (a) The ZFC heating and FC $M(T)$ curves of the single crystal of Gd_5Ge_4 measured at $H=0.5$ kOe. The inset is the ZFC magnetization difference between M_c and $M_a(M_b)$. (b) The $M(T)$ curves in the AFM state extracted from the $M(T)$ curves shown in Fig. 6.

During the second increase of the magnetic field, the magnetization follows the first demagnetization curve at 2 K (not shown in Figs. 1 and 2 for conciseness), signaling that the entire sample remains in the FM state, i.e., the field-induced AFM-FM transition is irreversible and once the FM phase is formed, it is stable at this temperature after removing the magnetic field. However, the magnetization curves at 4 K do not precisely follow the first demagnetization path. Above 4 K, a steplike ferromagnetic behavior is seen in low fields. The saturation magnetization of the low-field FM state, estimated as shown by the dashed lines in Figs. 1 and 2, decreases with temperature and nearly disappears at ~ 14 K,

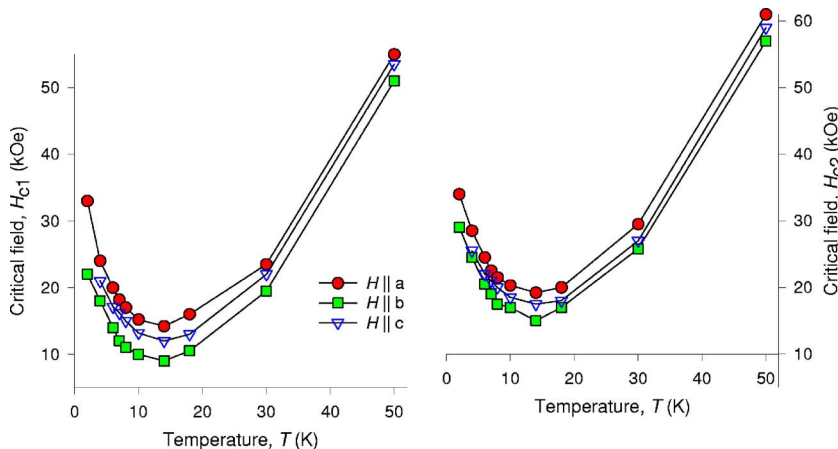


FIG. 9. (Color online) The anisotropy and temperature dependencies of the critical magnetic fields (H_{c1} , left and H_{c2} , right) of the AFM-FM transition in the ZFC single crystal of Gd_5Ge_4 .

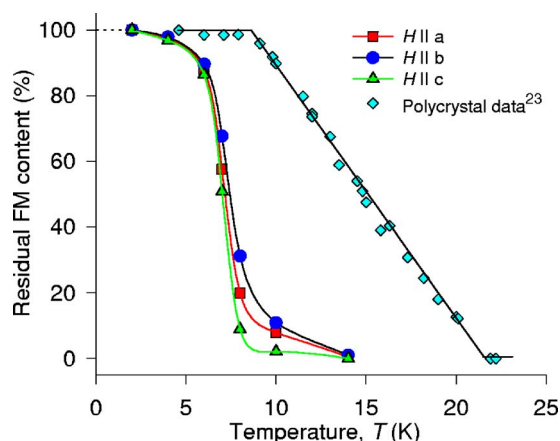


FIG. 10. (Color online) The temperature dependence of the amount of the residual FM phase in the single crystal of Gd_5Ge_4 after the first magnetization. The FM content is evaluated from the low field steps in the $M(H)$ curves by computing a ratio of the saturation magnetization at individual temperatures. The polycrystal data (Ref. 23) are shown for comparison.

pointing to the temperature associated with the minimum of H_{c1} and H_{c2} . Hence, between ~ 4 K and ~ 14 K, the first application of field induces the FM phase in the entire AFM sample. When the field is removed, a fraction of the sample volume is converted back into the AFM state, whereas the rest of the sample still remains in the FM state. That is, both the irreversible and reversible AFM-FM transformations coexist in this temperature range. Considering that dM/dH curves in the steplike magnetization region show no spin-flop anomaly below 7 K and that the AFM state involved in the AFM-FM transition along the c axis is the spin-flop AFM state, it is likely that the recovered AFM state is only the spin-flop AFM state below 7 K and a mixture of the normal and the spin-flop AFM states above 7 K. Above ~ 14 K, the $M(H)$ curves in the second application of field nearly coincide with those in the first field-increasing measurement because there is no residual FM phase after the first measurement cycle. Thus, the AFM-FM transition becomes fully reversible above ~ 14 K exhibiting directionally dependent hysteresis. We recall that a polycrystalline sample also shows a similar mix of reversibility and irreversibility of the AFM-FM transition, but the temperature range where the two types of transitions coexist is between ~ 10 K and ~ 20 K.^{18,23}

The residual contents of the FM phase along the three axes, evaluated from the low field magnetization steps in the second H -increasing $M(H)$ curves by computing a ratio of the saturation magnetization at individual temperatures, are illustrated in Fig. 10. The temperature dependencies of the residual FM phase content exhibit inverse S shapes, which is different when compared with a polycrystalline sample, where the residual FM content, derived by initially magnetizing the sample at 4.5 K by a 56 kOe field and then warming in a zero field up to the measurement temperature, varies linearly between ~ 10 K and ~ 21 K.²³ Notably, the residual FM amount also shows a directional dependence: between 4 K and 14 K, and especially from 7 to 10 K, it is the largest along the b axis and the smallest along the c axis. As a result,

the reversibility of the AFM-FM phase transition is best when the field is applied along the c axis and it is most incomplete when the magnetic field is applied parallel to the b axis. Different factors may play a role in the varying completion of the FM \rightarrow AFM transition upon removal of the magnetic field between 4 and 14 K. First, the maximum retention of the FM phase with the magnetic field applied along the b axis is consistent with this being the easy magnetization direction (see next paragraph). Second, the best reversibility with the magnetic field applied along the c axis is commensurate with the recovery of the normal AFM state occurring around 8.5 kOe in this temperature range [see Fig. 5(a)]. Finally, even though the domain structure of the ferromagnetic Gd_5Ge_4 is unknown, it is safe to assume that it is highly anisotropic and similar to that observed in a single crystal $\text{Gd}_5\text{Si}_2\text{Ge}_2$. The latter has the same crystal structure in the ferromagnetic state and exhibits stripe domains when viewed along the a axis, a rosette domain pattern typical of a soft uniaxial ferromagnet when viewed along the b axis, and practically no magnetic contrast when viewed along the c axis.³³

We now discuss the anisotropy of the FM-AFM transition based on the results described above. In Fig. 11 the H -decreasing $M(H)$ branches are compared at several temperatures. The magnetization always exhibits a rapid fall off at a certain critical field H_{c3} . Below ~ 4 K, the AFM-FM transition is irreversible and the FM \rightarrow AFM transition does not occur at all. The critical fields are anisotropic, i.e., H_{c3} (b axis) $< H_{c3}$ (a axis) $\cong H_{c3}$ (c axis). Since Gd_5Ge_4 is a collinear ferromagnet above H_{c3} , the same fields are expected to be the values where magnetization reaches saturation during the second field application at these temperatures. Therefore, the system exhibits a strong ferromagnetic anisotropy between the b axis and a or c axis, showing that the b axis is the easy magnetization direction in the FM state of Gd_5Ge_4 . The $M(H)$ curves nearly overlap with each other for the a axis and the c axis, showing no anisotropy between these two “hard magnetization” directions. Between ~ 4 K and 14 K, where a certain fraction of the sample preserves the FM state, the system shows behavior similar to that below 4 K. At and above 14 K, Gd_5Ge_4 maintains the notable anisotropy of the FM \rightarrow AFM transition that now starts at H_{c3} and ends at H_{c4} . The a -axis $M(H)$ demagnetization curve no longer overlaps with the c -axis $M(H)$ curve. The values of H_{c3} and H_{c4} remain the smallest along the b axis at temperatures as high as 30 K [Fig. 11(d)].

The anisotropy of the AFM-FM transition is also manifested in the $M(T)$ curves shown in Fig. 6. The 50 kOe $M(T)$ curves exhibit sharp FM-AFM transitions at $T_C = \sim 50$ K. The ZFC data and the FC data almost overlap showing little to no hysteresis, which is different from polycrystalline data, where a hysteresis of about ~ 8 K was observed.¹⁸ With magnetic field decreasing to 20 kOe, directionally dependent temperature hysteresis gradually sets in. The hysteresis is larger along the a axis than the other two axes, yet it always remains lower than that of a polycrystal. The ZFC $M(T)$ curves for the a and c axes exhibit an AFM \rightarrow FM transition followed by an FM \rightarrow AFM transition, while the FC $M(T)$ curves only exhibit an AFM \rightarrow FM transition and the sample

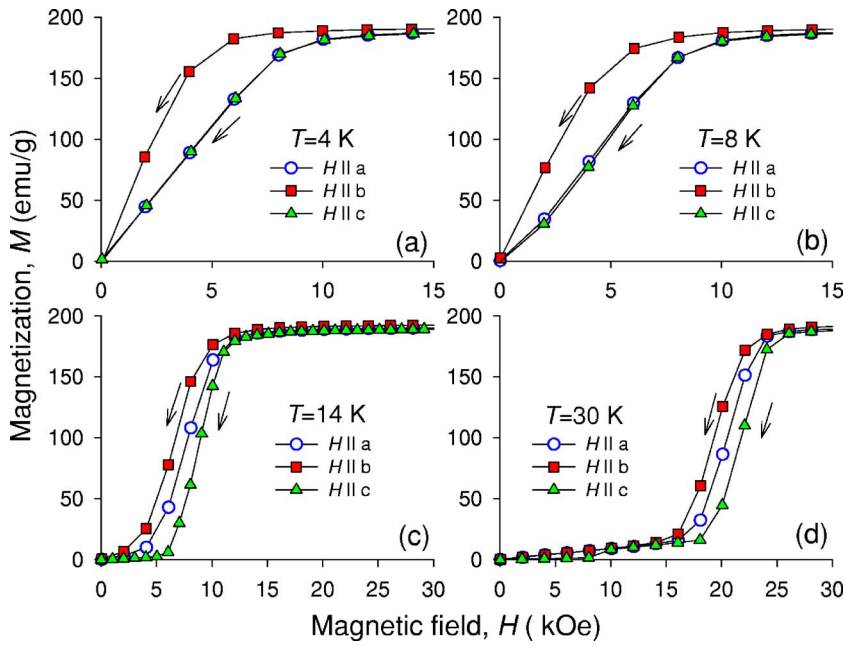


FIG. 11. (Color online) The H -decreasing $M(H)$ curves of the single crystal of Gd_5Ge_4 measured at $T=4$ K, 8 K, 14 K, and 30 K (see also Figs. 1 and 2).

remains in the FM state down to the lowest temperature, i.e., ~ 4 K. This is consistent with the isothermal magnetization results, where Figs. 1(a) and 2(a) show that the 20 kOe field is below H_{c1} of the low temperature $M(H)$ curves, thus the FM state cannot be induced by isothermally magnetizing the sample up to 20 kOe at 4 K along the a and c axes. As temperature increases beginning from 4 K, H_{c1} for these two directions lowers, soon becoming smaller than the 20 kOe field surrounding the sample, thus resulting in the temperature-induced AFM-FM transformation. The high temperature FM-AFM transition occurs when the critical magnetic fields begin to increase again above 14 K eventually exceeding 20 kOe. However, the 20 kOe ZFC $M(T)$ curve along the b axis shows only one high temperature FM-AFM transition. This can be related to the fact that the 20 kOe field is higher than H_{c1} between ~ 4 and 30 K. When $H=10$ kOe, the b -axis $M(T)$ curves still show AFM-FM and FM-AFM transitions, while the a - and c -axes $M(T)$ curves no longer show any FM state.

It is believed that the observed anisotropy is related to the anisotropy of the two crystal structures adopted by the Gd_5Ge_4 system in the AFM and FM states, both of which are layered with the layers extending in the ac plane that are stacked differently along the b axis. The arrangement of Gd atoms along the a and c axes is quite similar. Hence, it is feasible that in the spin-flop AFM state, the Gd moments remain ferromagnetically coupled within the layers but the interlayer coupling becomes AFM along the a axis. Hence, during the AFM-FM transition, the system changes its magnetic state from AFM coupling along the a axis to become a collinear ferromagnet along the c axis when the magnetic field is applied along this direction, whereas when the magnetic field is parallel to the a axis, the magnetic state is changed from the AFM state along the c axis to the collinear FM state along the a axis. In both cases, the Gd moments rotate within the ac plane without the involvement of the b axis. This feature results in the similarity of the anisotropy of

the FM state below 4 K, as seen in Fig. 11(a). The larger H_{c1} and H_{c2} along the a axis compared to the c axis (Fig. 9) is likely related to the anisotropy of the lattice constants and their variation during the AFM-FM transition, in which the value of a decreases from 7.68 Å in the AFM state to 7.54 Å in the FM state, while the value of c increases from 7.76 Å in the AFM state to 7.81 Å in the FM state at 6.1 K.²¹ The lattice expansion-related energy barrier between AFM and

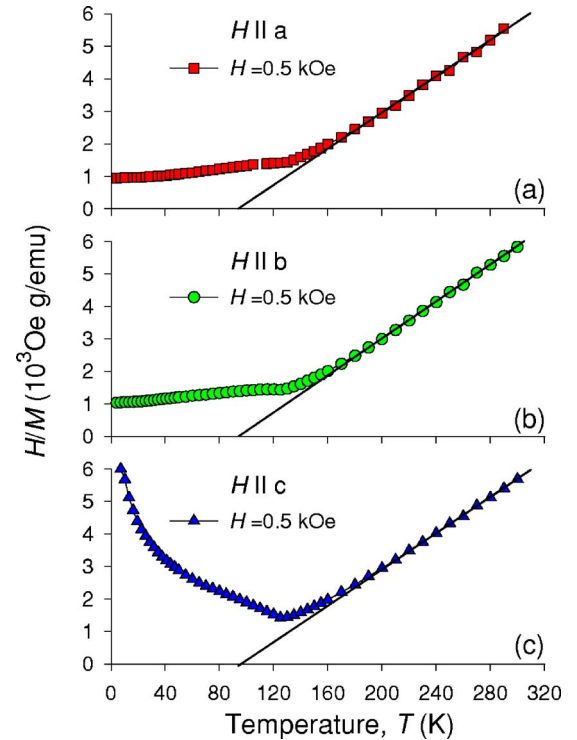


FIG. 12. (Color online) The temperature dependencies of the reciprocal magnetic susceptibility H/M of the Gd_5Ge_4 single crystal measured at $H=0.5$ kOe. The solid lines represent the Curie-Weiss fit.

FM states is larger for the a axis than for the c axis, leading to the larger H_{c1} and H_{c2} along the a axis [and to the smaller H_{c3} and H_{c4} along the same axis, see Figs. 11(b)–11(d)].

The arrangement of the Gd atoms along the b axis is quite different from the other two directions. When the magnetic field vector is applied along this axis, the system changes its magnetic state from AFM state along the c axis to the collinear FM state along the b axis, which is also quite different from the case when the field vector is parallel to the other two axes. The Ge–Ge bonds between the layers stacked along the b axis are broken before the AFM-FM transition and they become connected after the transition. The distinct uniqueness of the magnetic and crystal structures along the b axis defines this axis as the easy magnetization direction of the compound. In this direction, the free energy difference between the AFM state and FM state is likely smallest compared with the other two axes, which causes the smallest values of H_{c1} and H_{c2} along the b axis. Once the FM phase is formed in this direction, it is harder to be converted back into the AFM state (see Figs. 10 and 11). We, therefore, believe that the distinctly anisotropic mechanism of the martensitic-like structural transformation, which proceeds via the shear displacements of the slabs along the a axis and produces changes in both the chemical bonding and magnetic exchange interactions along the b axis (each slab shears along the a axis by as much as ~ 0.45 Å with respect to its nearest neighbor slab²¹), plays a significant role in bringing about the anisotropic features of the magnetization discussed above. We note that the magnetocrystalline anisotropy was also ob-

served in some other Gd-based materials, such as single crystals of Gd_2PdSi_3 ,⁵ Gd_2CuO_4 ,⁶ and GdCu_2 ,^{34,35} although the nature of the anisotropy in these compounds is likely different from that of Gd_5Ge_4 .

It is worth noting that consistent with the stability of the crystal structure of Gd_5Ge_4 , no anisotropy is found during the AFM-PM transition. Figure 12 shows the reciprocal magnetic susceptibility (H/M) at 0.5 kOe. All the curves follow Curie-Weiss law above ~ 160 K, showing no anisotropy (the paramagnetic Weiss temperatures, θ_p , are 94 K and the effective magnetic moments, p_{eff} , are $7.94 \mu_B/\text{Gd}$, in nearly ideal agreement with that of a free Gd^{3+} ion).

C. Magnetic phase diagrams

Based on the results presented above, we plot in Fig. 13 the magnetic phase diagrams along the three axes. The left panels [Figs. 13(a)–13(c)] are for the initial magnetization of the zero field cooled sample and, correspondingly, the right panels [Figs. 13(d)–13(f)] are for the second isothermal magnetization of the sample. As in the polycrystalline sample, T_N slowly decreases with increasing magnetic field. The values of H_{c1} and H_{c2} first decrease and then increase with the increasing temperature. Both exhibit a minimum around 14 K for the three axes. An extrapolation of the curves along each axis, shown by the dashed lines in Figs. 13(a)–13(c), results in a tricritical point with $H_{\text{tr}} = \sim 140$ kOe, above which the AFM state is completely suppressed, and $T_{\text{tr}} = \sim 90$ K. It is worth noting that a recent high field study of a low purity

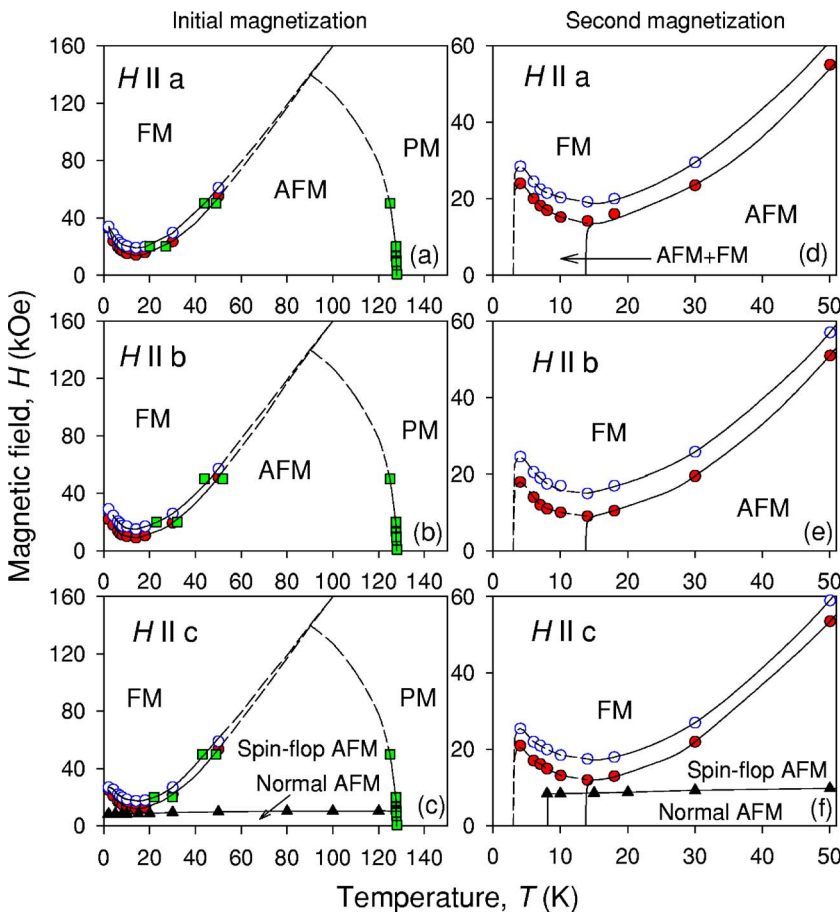


FIG. 13. (Color online) The H - T magnetic phase diagrams of single crystal of Gd_5Ge_4 along the three principal crystallographic axes, in which the symbols (\bullet) and (\circ) are the critical fields H_{c1} and H_{c2} , respectively, obtained from $M(H)$ curves, the symbols (\blacksquare) are the data derived from the $M(T)$ curves, and the symbols (\blacktriangle) are the data of H_{sf} . The plots on the left are for the initial magnetization of the ZFC single crystal. Extrapolations for magnetic fields exceeding 5 T shown by the dashed lines assume that both the AFM-FM and AFM-PM boundaries follow the corresponding boundaries established for polycrystalline Gd_5Ge_4 (Refs. 17 and 23). The plots on the right are for the second isothermal magnetization of the same crystal with only the low-temperature parts shown for clarity because above ~ 14 K the initial magnetization and the second magnetization diagrams are indistinguishable for the same direction.

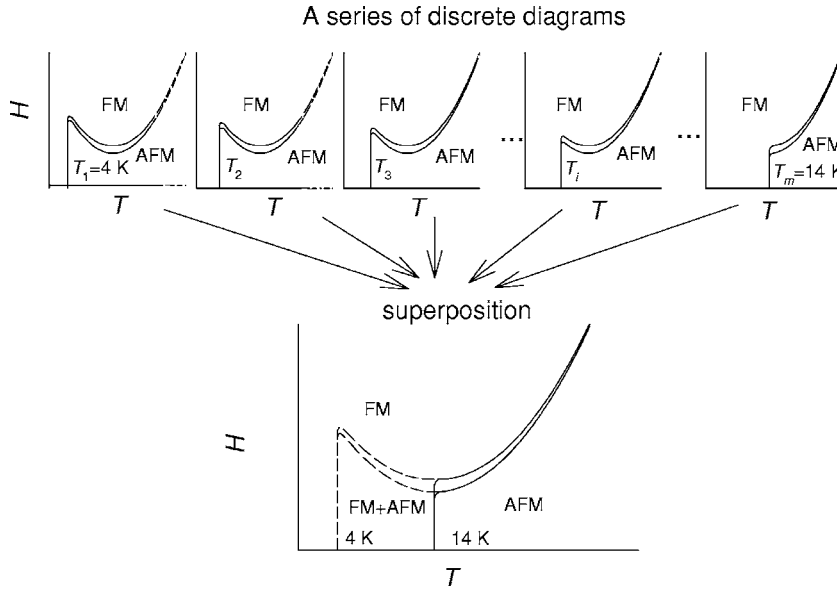


FIG. 14. A schematic of a second magnetization diagram (see the right-hand side of Fig. 13) as a superposition of a series of discrete diagrams with different AFM/FM termination boundaries at temperatures $4 \text{ K} < T_1 < T_2 < \dots < T_i < \dots < T_m = 14 \text{ K}$.

polycrystalline Gd_5Ge_4 sample by Casanova *et al.*³⁶ reported the same coordinates of the tricritical point: $H_{tcr} = \sim 140 \text{ kOe}$ and $T_{tcr} = \sim 90 \text{ K}$.

In the H - T diagrams representing the second magnetization, the AFM-PM transition boundary is the same as that of the initial magnetization and is hence omitted for clarity in Figs. 13(d)–13(f). The low-temperature parts in each of these three diagrams where the AFM state is partially recovered after the first application of the magnetic field can be regarded as a superposition of a series of discrete diagrams, which is illustrated in Fig. 14. In each of these diagrams, there is no coexistence of the AFM and FM states but the AFM phase region simply extends to a different lowest temperature, T_i ($i=1, 2, \dots, m$), where the AFM phase transforms into the FM phase isothermally. The result of the superposition is that between $\sim 4 \text{ K}$ and $\sim 14 \text{ K}$, there exists a mixture of FM and AFM states, as is observed experimentally. Considering that the amounts of the recovered FM phase vary as shown in Fig. 10, a fraction of the sample volume characterized by the diagrams where T_i is $\sim 6 \text{ K}$ to $\sim 8 \text{ K}$ is greater compared with diagrams having T_i between 4 K and 6 K and between 8 K and 14 K . This deviation from a monotonic distribution of T_i 's is likely associated with a peculiar microstructure^{37,38} and/or stress fields distributed anisotropically across the single crystal. We note that in the polycrystalline samples, the linear variation of the residual FM phase with temperature between $\sim 10 \text{ K}$ and $\sim 21 \text{ K}$ (Refs. 18 and 23) suggests that the sample fraction matching each discrete diagram is the same, as is expected for a polycrystal with a large number of randomly oriented and sized crystallites. In addition, according to Chattopadhyay *et al.*,³⁰ the kinetics of the AFM-FM transition is arrested at low temperatures, thus the residual FM state shown in Fig. 10 may actually be the trapped FM state. Obviously, the effect of kinetic arrest, if any, of the AFM-FM transition is weaker in the single crystal (starts at $\sim 14 \text{ K}$) than in the polycrystal (starts at $\sim 21 \text{ K}$). Note that temperatures at which the kinetic arrest develops are different although the range of temperatures over which the system becomes completely arrested is nearly identical

($\sim 10 \text{ K}$ for the single crystal and $\sim 11 \text{ K}$ for the polycrystal). In the single crystal, the FM phase is arrested very rapidly when temperature is reduced to $\sim 8 \text{ K}$, while the trapping process in the polycrystal is much more gradual, which correlates with the simpler Sm_5Ge_4 -type (AFM)/ Gd_5Si_4 -type (FM) domain structure in the single crystal compared to the polycrystal.

The anisotropy of the phase diagram is noticeable (see also Fig. 9). The values of H_{c1} and H_{c2} along the three axes are different at the same temperature. The AFM state with field along the c axis is divided into two regions—normal AFM and spin-flop AFM states. From the H - T diagram of the initial magnetization [Fig. 13(c)], when $T < T_N$, the spin-flop transition from the normal AFM state to the spin-flop AFM state can be observed in the $M(H)$ curves along the c axis. The spin-flop transition can be also observed in the $M(T)$ curves when $8.3 \text{ kOe} < H < 10.3 \text{ kOe}$. From the H - T diagram of the second magnetization [Fig. 13(f)], the spin-flop transition can be only observed in the temperature range $7 \text{ K} < T < T_N$ in the $M(H)$ curves. When $4 \text{ K} < T < 7 \text{ K}$, the residual AFM state is only retained in the spin-flop AFM state. Therefore, the increase of the reversibility of the AFM-FM transition with temperature increases the content of normal AFM phase.

IV. CONCLUSIONS

A reversible spin-flop transition along the c axis occurs in a single crystal of Gd_5Ge_4 at various magnetic fields (8.3 kOe – 10.3 kOe) and temperatures (2 K – 128 K), which is not observed when the field is applied along the a and b axes. This anisotropy can be understood by considering the configuration of the Gd moments in the AFM state with respect to the magnetic field vector. In the normal AFM state, the configuration of the Gd moments along the c axis is different from the AFM state along the a and b axes. Increasing temperature reduces the magnetization difference between these axes, and thus, reduces the anisotropy of the AFM state. In the spin-flop AFM state, the configuration of

the Gd moments along the c axis becomes similar to that along the a and b axes in the normal AFM state, resulting in the similarity of the magnetic properties in the AFM state. Thus, increasing the magnetic field effectively decreases the anisotropy of the AFM state. The fully irreversible AFM-FM transition is observed at low temperatures (below ~ 4 K); above ~ 14 K, the same transformation becomes fully reversible. Between ~ 4 and ~ 14 K there is a mixture of both transitions. The resultant residual FM content is larger for the b axis than for the a and c axes at the same temperature, and accordingly, the critical field for the AFM-FM transition along the b axis is smaller than that along the other two axes. In the FM state, the b axis is the easy magnetization direction

of the compound. The anisotropy of the AFM-FM transition is consistent with the anisotropic features of the distinctly layered crystal structures of the two polymorphic modifications of the compound despite negligible single ion anisotropy of the Gd^{3+} ion. The magnetic phase diagrams exhibit clear anisotropy.

ACKNOWLEDGMENTS

The Ames Laboratory is operated for the U.S. Department of Energy by Iowa State University. This work was supported by the Office of Basic Energy Sciences, Materials Sciences Division of the U.S. Department of Energy under Contract No. W-7405-ENG-82.

*Corresponding author. Email address: vitkp@ameslab.gov

- ¹Jong-Soo Rhyee, B. K. Cho, and H. C. Ri, *J. Appl. Phys.* **93**, 8346 (2003).
- ²M. Okazaki, N. Tanaka, and K. Motizuki, *J. Appl. Phys.* **87**, 4876 (2000).
- ³G. Uimin and W. Brenig, *Phys. Rev. B* **61**, 60 (2000).
- ⁴M. D. Kuzmin, *Phys. Rev. B* **51**, 8904 (1995).
- ⁵S. R. Saha, H. Sugawara, T. D. Matsuda, H. Sato, R. Mallik, and E. V. Sampathkumaran, *Phys. Rev. B* **60**, 12162 (1999).
- ⁶A. Butera, M. Tovar, S. B. Oseroff, and Z. Fisk, *Phys. Rev. B* **52**, 13444 (1995).
- ⁷V. K. Pecharsky and K. A. Gschneidner, Jr., *Phys. Rev. Lett.* **78**, 4494 (1997).
- ⁸V. K. Pecharsky and K. A. Gschneidner, Jr., *Appl. Phys. Lett.* **70**, 3299 (1997).
- ⁹L. Morellon, P. A. Algarabel, M. R. Ibarra, J. Blasco, B. García-Landa, Z. Arnold, and F. Albertini, *Phys. Rev. B* **58**, R14721 (1998).
- ¹⁰L. Morellon, J. Stankiewicz, B. García-Landa, P. A. Algarabel, and M. R. Ibarra, *Appl. Phys. Lett.* **73**, 3462 (1998).
- ¹¹E. M. Levin, V. K. Pecharsky, and K. A. Gschneidner, Jr., *Phys. Rev. B* **60**, 7993 (1999).
- ¹²W. Choe, V. K. Pecharsky, A. O. Pecharsky, K. A. Gschneidner, Jr., V. G. Young, Jr., and G. J. Miller, *Phys. Rev. Lett.* **84**, 4617 (2000).
- ¹³V. K. Pecharsky and K. A. Gschneidner, Jr., *Adv. Mater. (Weinheim, Ger.)* **13**, 683 (2001).
- ¹⁴L. Morellon, J. Blasco, P. A. Algarabel, and M. R. Ibarra, *Phys. Rev. B* **62**, 1022 (2000).
- ¹⁵C. Magen, Z. Arnold, L. Morellon, Y. Skorokhod, P. A. Algarabel, M. R. Ibarra, and J. Kamarad, *Phys. Rev. Lett.* **91**, 207202 (2003).
- ¹⁶V. K. Pecharsky and K. A. Gschneidner, Jr., *J. Alloys Compd.* **260**, 98 (1997).
- ¹⁷E. M. Levin, V. K. Pecharsky, K. A. Gschneidner, Jr., and G. J. Miller, *Phys. Rev. B* **64**, 235103 (2001).
- ¹⁸E. M. Levin, K. A. Gschneidner, Jr., and V. K. Pecharsky, *Phys. Rev. B* **65**, 214427 (2002).
- ¹⁹C. Magen, L. Morellon, P. A. Algarabel, C. Marquina, and M. R. Ibarra, *J. Phys.: Condens. Matter* **15**, 2389 (2003).
- ²⁰F. Casanova, A. Labarta, X. Batlle, J. Marcos, L. Mañosa, A. Planes, and S. de Brion, *Phys. Rev. B* **69**, 104416 (2004).
- ²¹V. K. Pecharsky, A. P. Holm, K. A. Gschneidner, Jr., and R. Rink,

- Phys. Rev. Lett.* **91**, 197204 (2003).
- ²²Ya. Mudryk, A. P. Holm, K. A. Gschneidner, Jr., and V. K. Pecharsky, *Phys. Rev. B* **72**, 064442 (2005).
- ²³H. Tang, V. K. Pecharsky, K. A. Gschneidner, Jr., and A. O. Pecharsky, *Phys. Rev. B* **69**, 064410 (2004).
- ²⁴F. Casanova, A. Labarta, and X. Batlle, *Phys. Rev. B* **72**, 172402 (2005).
- ²⁵E. M. Levin, K. A. Gschneidner, Jr., T. A. Lograsso, D. L. Schlagegel, and V. K. Pecharsky, *Phys. Rev. B* **69**, 144428 (2004).
- ²⁶L. Tan, A. Kreyssig, J. W. Kim, A. I. Goldman, R. J. McQueeney, D. Wermeille, B. Sieve, T. A. Lograsso, D. L. Schlagegel, S. L. Budko, V. K. Pecharsky, and K. A. Gschneidner, Jr., *Phys. Rev. B* **71**, 214408 (2005).
- ²⁷D. L. Schlagegel, T. A. Lograsso, A. O. Pecharsky, and J. A. Sampaio, in *Light Metals 2005*, edited by H. Kvande (The Minerals, Metals and Materials Society, Warrendale, PA, 2005), p. 1177.
- ²⁸Materials Preparation Center, Ames Laboratory U.S. DOE, Ames, IA, USA, www.mpc.ameslab.gov
- ²⁹V. Hardy, S. Majumdar, S. Crowe, M. R. Lees, D. McK. Paul, L. Hervé, A. Maignan, S. Hébert, C. Martin, C. Yaicle, M. Hervieu, and B. Raveau, *Phys. Rev. B* **69**, 020407(R) (2004).
- ³⁰M. K. Chattopadhyay, M. A. Manekar, A. O. Pecharsky, V. K. Pecharsky, K. A. Gschneidner, Jr., J. Moore, G. K. Perkins, Y. V. Bugoslavsky, S. B. Roy, P. Chaddah, and L. F. Cohen, *Phys. Rev. B* **70**, 214421 (2004).
- ³¹M. K. Chattopadhyay, M. A. Manekar, A. O. Pecharsky, V. K. Pecharsky, K. A. Gschneidner, Jr., J. Moore, G. K. Perkins, Y. V. Bugoslavsky, S. B. Roy, P. Chaddah, and L. F. Cohen (unpublished).
- ³²L. Néel, *Ann. Phys.* **5**, 232 (1936).
- ³³J. S. Leib, C. C. H. Lo, J. E. Snyder, D. C. Jiles, V. K. Pecharsky, D. S. Schlagegel, and T. A. Lograsso, *IEEE Trans. Magn.* **38**, 2447 (2002).
- ³⁴M. Rotter, M. Doerr, M. Loewenhaupt, A. Lindbaum, H. Muller, J. Enser, and E. Gratz, *J. Magn. Magn. Mater.* **236**, 267 (2001).
- ³⁵M. Rotter, M. Loewenhaupt, M. Doerr, A. Lindbaum, and H. Michor, *Phys. Rev. B* **64**, 014402 (2001).
- ³⁶F. Casanova, S. de Brion, A. Labarta, and X. Batlle, *J. Phys. D* **38**, 3343 (2005).
- ³⁷J. Szade, G. Skorek, and A. Winiarski, *J. Cryst. Growth* **205**, 289 (1999).
- ³⁸O. Ugurlu, L. S. Chumbley, D. L. Schlagegel, and T. A. Lograsso, *Acta Mater.* **54**, 1211 (2006).